International Journal of Digital Earth
Publication details, including instructions for authors and subscription information:
http://www.tandfonline.com/loi/tjde20

Seasonal dynamic pattern analysis on global FPAR derived from AVHRR GIMMS NDVI

Dailiang Peng [a b], Bing Zhang [a b], Liangyun Liu [a b], Dongmei Chen [c], Hongliang Fang [d] & Yong Hu [a]

[a] Center for Earth Observation and Digital Earth, Chinese Academy of Sciences, Beijing, China

[b] Key Laboratory of Digital Earth, Chinese Academy of Sciences, Beijing, China

[c] Department of Geography, Queen's University, Kingston, ON, Canada

[d] LREIS, Institute of Geographic Sciences and Natural Resources Research, Chinese Academy of Sciences, Beijing, China

Published online: 18 Aug 2011.

To cite this article: Dailiang Peng, Bing Zhang, Liangyun Liu, Dongmei Chen, Hongliang Fang & Yong Hu (2012) Seasonal dynamic pattern analysis on global FPAR derived from AVHRR GIMMS NDVI, International Journal of Digital Earth, 5:5, 439-455, DOI: 10.1080/17538947.2011.596579

To link to this article: http://dx.doi.org/10.1080/17538947.2011.596579

International Journal of Digital Earth,
Vol. 5, No. 5, September 2012, 439–455

Taylor & Francis
Taylor & Francis Group

Seasonal dynamic pattern analysis on global FPAR derived from AVHRR GIMMS NDVI

Dailiang Peng[a,b], Bing Zhang[a,b]*, Liangyun Liu[a,b], Dongmei Chen[c], Hongliang Fang[d] and Yong Hu[a]

[a]*Center for Earth Observation and Digital Earth, Chinese Academy of Sciences, Beijing, China;* [b]*Key Laboratory of Digital Earth, Chinese Academy of Sciences, Beijing, China;* [c]*Department of Geography, Queen's University, Kingston, ON, Canada;* [d]*LREIS, Institute of Geographic Sciences and Natural Resources Research, Chinese Academy of Sciences, Beijing, China*

(*Received 22 February 2011; final version received 9 June 2011*)

The purpose of this paper is to develop Advanced Very High Resolution Radiometer (AVHRR) Global Inventory Modelling and Mapping Studies (GIMMS) Normalised Difference Vegetation Index (NDVI; AVHRR GIMMS NDVI for short) based fraction of absorbed photosynthetically active radiation (FPAR) from 1982 to 2006 and focus on their seasonal and spatial patterns analysis. The available relationship between FPAR and NDVI was used to calculate FPAR values from 1982 to 2006 and validated by Moderate-resolution Imaging Spectroradiometer (MODIS) FPAR product. Then, the seasonal dynamic patterns were analysed, as well as the driving force of climatic factors. Results showed that there was an agreement between FPAR values from this study and those of the MODIS product in seasonal dynamic, and the spatial patterns of FPAR vary with vegetation type distribution and seasonal cycles. The time series of average FPAR revealed a strong seasonal variation, regular periodic variations from January 1982 to December 2006, and opposite patterns between the Northern and Southern Hemispheres. Evergreen vegetation FPAR values were close to 0.7. A clear single-peak curve was observed between 30°N and 80°N – an area covered by deciduous vegetation. In the Southern Hemisphere, the time series fluctuations of FPAR averaged by 0.7° latitude zones were not clear compared to those in the Northern Hemisphere. A significant positive correlation ($P < 0.01$) was observed between the seasonal variation of temperature and precipitation and FPAR over most other global meteorological sites.

Keywords: global FPAR; seasonal pattern; AVHRR GIMMS NDVI

1. Introduction

From 1980 to the present, the Earth has experienced dramatic environmental changes, especially in the global climate. The patterns of terrestrial ecosystem variables associated with climate change have been widely considered by scientists (Ruimy *et al.* 1994, Sellers *et al.* 1996, Nemani *et al.* 2003, Liu *et al.* 2006). Fraction of absorbed photosynthetically active radiation (FPAR), which is generally defined as the fraction of photosynthetically active radiation (PAR) absorbed by vegetation in the 0.4–0.7 μm spectrum, has been identified as one of several key terrestrial products. FPAR excludes the fraction of incident PAR reflected from the canopy and

*Corresponding author. Email: zb@ceode.ac.cn

ISSN 1753-8947 print/ISSN 1753-8955 online

http://dx.doi.org/10.1080/17538947.2011.596579
http://www.tandfonline.com

the fraction absorbed by the soil surface, but includes the portion of PAR reflected by the soil/understory and absorbed by the canopy on its return to space (McCallum *et al.* 2010). FPAR characterises vegetation canopy function and its energy absorption capacity and is required to describe the exchange of fluxes of energy, mass and momentum between the surface and the atmosphere. FPAR is one of the key parameters in many ecosystem productivity models (e.g. production efficiency models), as well as global models of climate, hydrology, biogeochemistry and ecology (Sellers *et al.* 1996).

Spatiotemporal patterns are important features of any FPAR dataset (McCallum *et al.* 2010). Several global FPAR datasets are available through remote sensing methods, such as those provided by the Moderate-resolution Imaging Spectroradiometer (MODIS), the Multi-angle Imaging SpectroRadiometer (MISR; March 2000 to present), the Carbon Cycle and Change in Land Observational Products from an Ensemble of Satellites (CYCLOPES; 1999 to 2007), the Joint Research Center (JRC; 1997 to 2006) and GLOBCARBON (1998 to 2006). The time series of existing FPAR products are not long enough to study the relationship between vegetation dynamics and global climate change or other anthropogenic activities. A global monthly 0.5° FPAR dataset has been generated from the AVHRR Pathfinder Land NDVI from July 1981 to May 2001 based on radiative transfer models (Myneni *et al*. 1997). Unfortunately, this dataset is no longer available to the public. Several regional or short-term studies of FPAR spatiotemporal patterns have been conducted (Myneni *et al.* 2002, Fensholt *et al.* 2004, Gobron *et al.* 2006), but a global, long-term comprehensive analysis of FPAR on seasonal dynamics and their response to climate change is lacking. Therefore, a longer-term consistent FPAR product is needed for studying the spatiotemporal dynamics of global vegetation and their response to climate change; this is the focus of this paper.

There are two types of models used for estimating FPAR. Bottom-up models often use highly complex ecosystem simulation models to describe the detailed interaction among the incoming radiation, individual leaves and the canopy as a whole. These models often require a number of input variables, which can be difficult to derive (Fensholt 2004). Top-down statistical models rely on the spectral features of the observations to routinely deliver FPAR through a semi-empirical relationship linking the variables of interest to a combination of radiometric measurements (i.e. vegetation index; Gobron *et al.* 1999; Buermann *et al.* 2002; Bacour *et al.* 2006). Parametric models represent complex photosynthetic processes using a few biophysical variables (Fensholt *et al.* 2004). Theoretically, most of these models originate from the light use efficiency (LUE) concept proposed by Monteith (1972) and seek to describe light absorption by plant canopies through the relationship between the Normalised Difference Vegetation Index (NDVI) and FPAR (Hanan *et al.* 1995; Le Roux *et al*. 1997). Many studies showed a linear or approximately linear relationship between NDVI and FPAR (Ruimy *et al.* 1994, Myneni *et al.* 1995, 2002). Hatfield *et al.* (1984) found a linear relationship for wheat. Few studies have, however, tested the relationship against in situ measurements (Fensholt *et al.* 2004), and Le Roux *et al.* (1997) found the relation to be non-linear for humid savannah grassland. A number of factors were found to influence the parameters of this linear relation; most of them are canopy-related factors, especially for vegetation morphology, which varies widely among different land covers (Potter *et al.* 1999, Fensholt *et al.* 2004). Based on the theoretical relation between FPAR and simple

ratio vegetation index (SR), a simple transformation of NDVI, Sellers *et al.* (1992) confirmed the near-linearity relationship by analysing the field data over a range of spatial scales; FPAR for different land covers were estimated with different NDVI thresholds (Sellers *et al.* 1996).

This paper extends and adapts the NDVI-based approach as used in Sellers *et al.* (1996) to derive FPAR from GIMMS NDVI SR FPAR and analyse the time series pattern of global FPAR from 1982 to 2006. The paper is organised as follows. In the following section, we describe the methods used to estimate global FPAR from 1982 to 2006 and analyse seasonal patterns of global FPAR. Results and discussion are reported in Section 3 in four parts: comparisons with MODIS FPAR, geographical and seasonal patterns, time series variations of global FPAR, and the relationship with two climate factors (temperature and precipitation). Finally, the concluding remarks and limitations are summarised in Section 4.

2. Methodology

2.1 FPAR estimation

Sellers *et al.* (1992) provided a strong mechanistic basis for building a correlation between FPAR and the associated simple ratio vegetation index (SR) and this relation is given as follows (Sellers *et al.* 1996).

$$\mathrm{FPAR} = \min\left\{\frac{(\mathrm{SR}-\mathrm{SR}_{\min})(FPAR_{\max}-FPAR_{\min})}{\mathrm{SR}_{\max}-\mathrm{SR}_{\min}}+FPAR_{\min}, FPAR_{\max}\right\}$$

where:

$\mathrm{SR} = (1+\mathrm{NDVI})/(1-\mathrm{NDVI})$;
$\mathrm{FPAR}_{\max} = 0.95$;
$\mathrm{FPAR}_{\max} = 0.001$;
$\mathrm{FPAR}_{\max}$, $\mathrm{FPAR}_{\min}$ independent of vegetation type;
$\mathrm{SR}_{\max}$ = SR value corresponding tp 98% of NDVI;
$\mathrm{SR}_{\min}$ = SR value corresponding tp 5% of NDVI.

In this study, GIMMS NDVI datasets from 1982 to 2006 are used, which are composited at a 15-day time step, the 15a composite is the maximum value composite from the first 15 days of the month, and the second (15b) is from days 16 through the end of the month. The data are given in an 8 km Albers Equal Area Conic projection, Clarke 1866 ellipsoid, and in geographic coordinates, WGS84 datum. New features of this dataset include reduced NDVI variations arising from calibration, view geometry, volcanic aerosols, satellite drift and other effects not related to actual vegetation change. The tests on sites showed reasonable agreement of inter-annual variation in GIMMS NDVI and other measures of vegetation, and the variation in GIMMS NDVI is realistic on specific sites (Davenport and Nicholson 1993, Malmstrom *et al.* 1997, D'Arrigo *et al.* 2000). The data and its guide are available for free via http://glcf.umiacs.umd.edu/data/gimms/ (Tucker *et al.* 2005).

The SR_{max} and SR_{min} vary with vegetation types. The Globcover land cover product at 300 m resolution for the period December 2004 to June 2006 is involved in the calculation of different vegetation types' FPAR, which was derived by the classification of a Medium Resolution Imaging Spectrometer Instrument (MERIS) Full Resolution (FR) time series. Its 22 land cover classes are defined with the UN Land Cover Classification System (LCCS). Using the 4258-point Globcover validation dataset, the final accuracy results showed the quality of this global product was quite satisfactory (Bicheron *et al.* 2008a). A complete description of format and content of the Globcover surface reflectance mosaics is given in the product description manual (Bicheron *et al.* 2008b), and the Globcover products are made available to the public by the Pôle d'Observation des Surfaces Terrestres aux Echelles Larges (POSTEL) Service Centre with the agreement of the European Space Agency (ESA) and can be downloaded from http://www.esa.int/due/ionia/globcover. Corresponding to the new Simple Biosphere model (SiB2) vegetation classification (Sellers *et al.* 1996), 22 land cover classes from Globcover were recombined to nine vegetation types (Figure 1). The 98% NDVI for tall vegetation types is assumed to represent vegetation at full cover and maximum activity with an FPAR value close to 1 (here assumed to be 0.950). The 5% desert value is assumed to represent no vegetation activity and an FPAR value of 0.001 for all land cover types (Sellers *et al.* 1996). Globcover pixels were re-projected to AVHRR GIMMS NDVI coordinates with an 8 km spatial resolution. We calculated the percentages of land cover types in an 8×8 km area and the main land cover type was used as the new land cover type in 8 km pixels, and the land cover type-dependent NDVI values for 98% and 5% were calculated in Table 1.

2.2 Seasonal pattern analysis of Global FPAR

After global FPAR was estimated by the above method, the MODIS standard FPAR product was used to validate the accuracy of GIMMS NDVI SR FPAR. Considering the Globcover land cover product for FPAR calculation was obtained during the period December 2004 to June 2006, we may isolate the influence of land cover

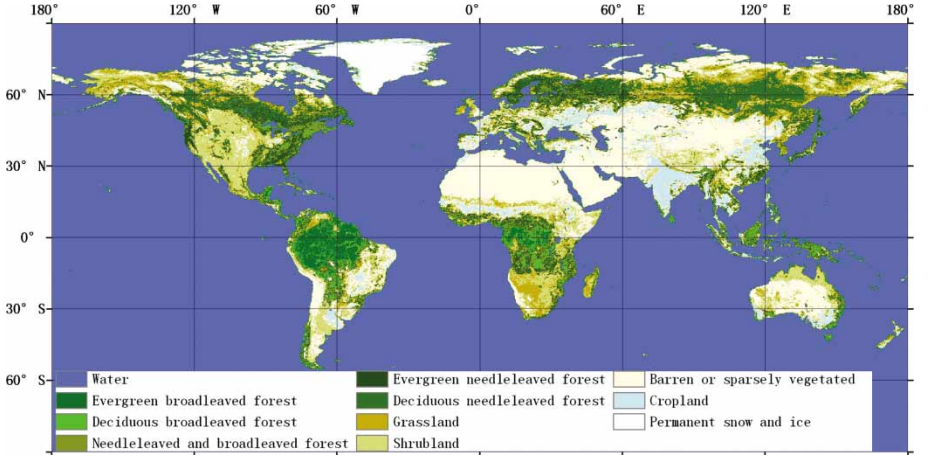

Figure 1. Global land cover map.

Table 1. Ninety-eight percent and 5% NDVI and corresponding SR values for different vegetation types.

Vegetation type	$NDVI_{5\%}$	SR_{min}	$NDVI_{98\%}$	SR_{max}
Evergreen broadleaved forest	0.245	1.649	0.850	12.333
Deciduous broadleaved forest	0.165	1.395	0.845	11.903
Needleleaved and broadleaved forest	0.115	1.260	0.865	13.815
Evergreen needleleaved forest	0.13	1.299	0.815	9.811
Deciduous needleleaved forest	0.001	1.002	0.840	11.500
Grassland	0.045	1.094	0.760	7.333
Shrubland	0.105	1.235	0.780	8.091
Barren or sparsely vegetated area	0.02	1.041	0.690	5.452
Cropland	0.13	1.299	0.795	8.756

change when comparing two datasets in 2006. Also, Eurasia includes almost every type of vegetation, so we compared two FPAR datasets in Eurasia in 2006. First, MODIS standard FPAR products were re-projected from the Sinusoidal Projection to Albers Equal Area Conic projection and geographic coordinates with 8 km spatial resolution. Then we averaged both FPAR datasets monthly over the entire Eurasia region by land cover type and their seasonal patterns were compared.

The FPAR geographical and temporal patterns including FPAR spatial (including the Northern and Southern Hemisphere) and seasonal distributions and their relationship with vegetation distribution are considered in this paper. We gave the distribution of global FPAR in four mid-seasonal months (January, April, July and October), in order to explore the seasonal characteristics of global FPAR. Second, the multi-year (1982–2006) mean seasonal FPAR values across all vegetation types were graphed separately, and the time series variation from January 1982 to December 2006 was mapped at a latitudinal scale in the Northern and Southern Hemisphere.

The three most ecologically important environmental factors affecting rangeland plant growth are light, temperature and water (precipitation). Light is the most important ecological factor, which is necessary for photosynthesis and plant growth (Llewellyn 2004). Precipitation and temperature directly influence water balance, causing changes in the soil moisture regime that, in turn, influences plant growth and temperature also affects plant phenology and growth directly (Wang *et al.* 2003). Many studies have found that there are lead/lag correlations between climate factors and vegetation variables, such as NDVI, EVI, NPP and FPAR (Wang *et al.* 2003, Liu *et al.* 2006, Notaro *et al.* 2006, Peng *et al.* 2008, Peng *et al.* 2010). Notaro *et al.* (2006) confirmed that the maximum correlation between FPAR and climate factors occurred at zero lag. The Global Historical Climatology Network (GHCN-Monthly) database contains historical temperature and precipitation for thousands of land stations worldwide, and the data are available without charge through the National Climatic Data Center (NCDC) anonymous FTP service at http://www.ncdc.noaa.gov/ghcnm/v2.php (Peterson and Vose 1997, Peterson *et al.* 1998). The monthly mean temperature and accumulated precipitation with more than 20 years records from 1982 to 2006 were selected from the GHCN-Monthly Version 2 dataset to examine relations between climate factors (temperature and precipitation) and

FPAR across the station locations over the entire period from 1982 to 2006. The correlation coefficients were calculated and then the significant levels were examined.

3. Results and discussion

3.1 Comparisons with MODIS FPAR

The seasonal variations of FPAR values throughout a year for different biomes are displayed in Figure 2. It was found that the GIMMS NDVI SR FPAR showed consistent seasonal variations with MODIS FPAR across all land cover types. Evergreen forest FPAR from both datasets had a smaller seasonal variation, especially for evergreen broadleaf forest. However, FPAR values of other vegetation showed significant seasonal variation and the largest value appeared in July.

The statistical results of difference between MODIS FPAR and AVHRR based FPAR showed that: in Eurasia, the percentages of absolute errors less than 0.01, 0.05 and 0.1 were 10.65%, 30.23% and 56.6%, respectively, and in more than 70% of areas, MODIS FPAR values are larger than AVHRR based FPAR, especially for the forest vegetation, with the difference ranging from 0.0 to 0.35.

Gao (2000) confirms that because of differences in channel positions and widths between MODIS and AVHRR, the largest bias comes from the near infrared and red channels, and which caused the systematic bias between MODIS and AVHRR NDVI. In addition, GIMMS NDVI had no atmospheric correction in the processing streams, and relied solely on Maximum Value Composite (MVC) to reduce the effects of changes in atmospheric properties (Nagol *et al.* 2009). However, the temporal compositing technique (such as MVC) is of limited use in short compositing periods (El Saleous *et al.* 2000). All those may contribute to the difference between MODIS FPAR and AVHRR based FPAR in this study.

The differences between GIMMS NDVI SR FPAR and MODIS FPAR are greater for the densest canopies than other vegetation types. Several studies have pointed out the tendency of the MODIS FPAR product to overestimate actual FPAR, in the case of mixed stands and dense canopies. The high MODIS FPAR values are overestimated by 0.06–0.15 (approximately 8–20%) (Cohen *et al.* 2003, Wang *et al.* 2004, Fang *et al.* 2005, Huemmrich *et al.* 2005, Bacour *et al.* 2006). In addition, Huete (1988) found that AVHRR NDVI exhibited saturated signals for high biomass conditions, such as densely vegetated, forested areas, which may also partly contribute to the low value of GIMMS NDVI SR FPAR in this study for forest regions.

3.2 Seasonal and geographical distributions

Figure 3 shows Global FPAR for January, April, July and October averaged from 1982 to 2006 as calculated using the method in Section 2.1 (the areas in Greenland covered by snow or ice were coloured blue as water). We compared the global spatial distribution of the 25-year average FPAR with the global land cover and found that the global spatial distribution FPAR is primarily determined by the land cover types and growth season. Therefore, the largest FPAR values are found in forest areas during local summer, except for the tropical regions around the Equator with evergreen vegetation.

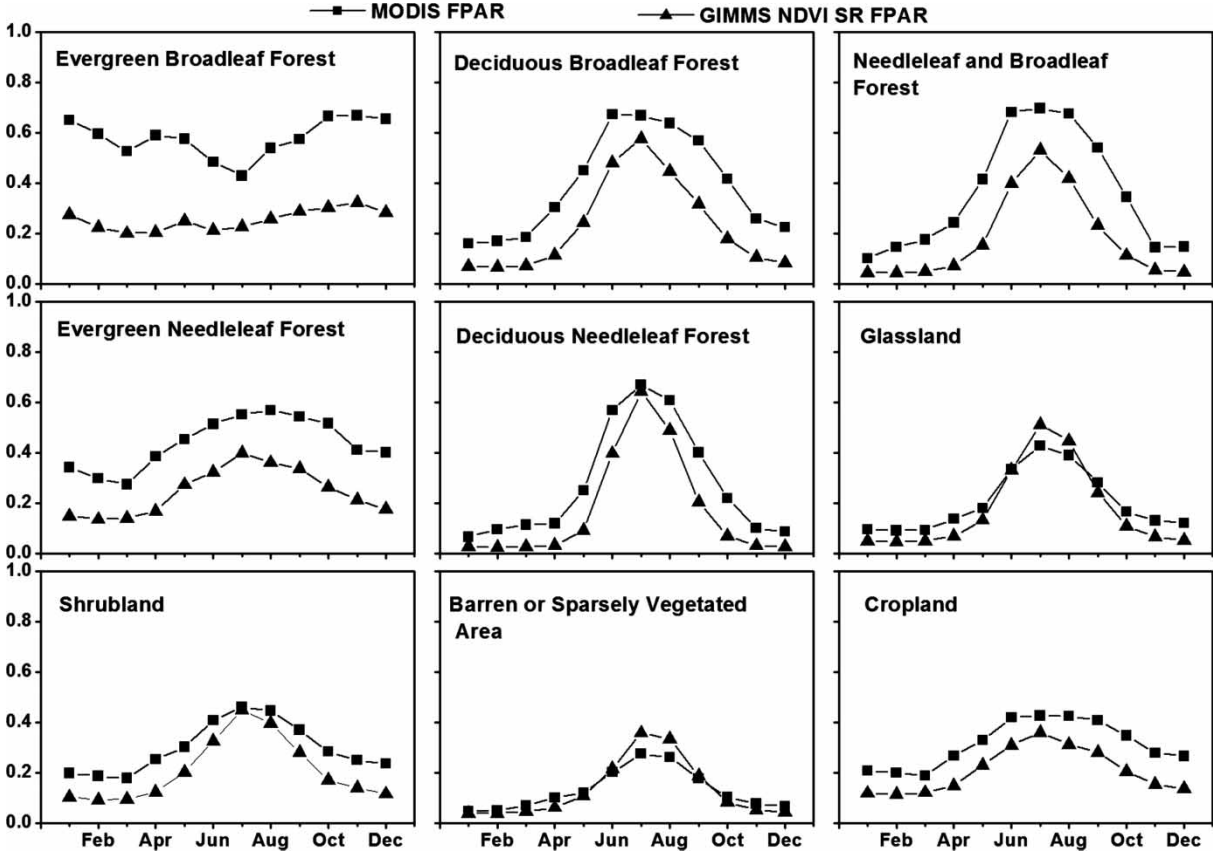

Figure 2. Comparison of monthly mean values from two FPAR datasets over Eurasia for the year 2006 by land cover type.

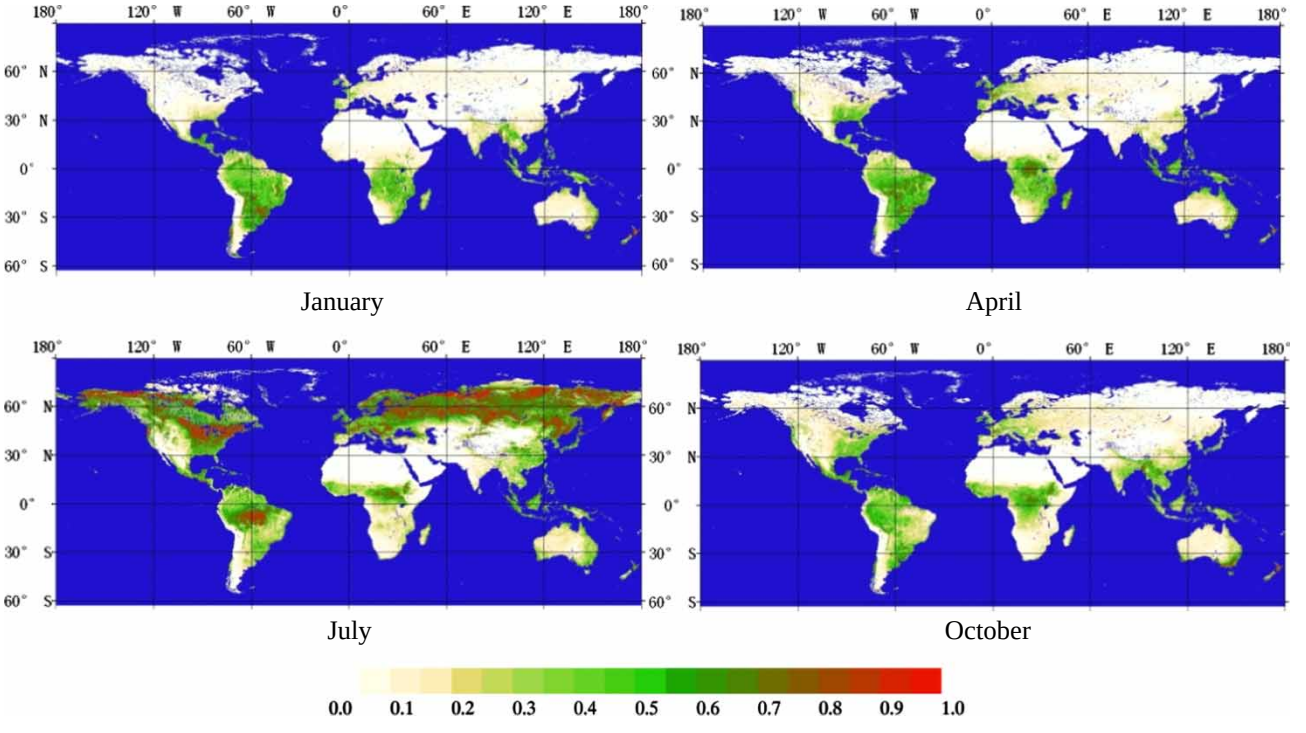

Figure 3. Long-term (1982–2006) average distribution of GIMMS NDVI SR global FPAR for the mid-seasonal months of January, April, July and October.

In the Northern Hemisphere, FPAR increases from January to a maximum in July and then decreases towards October (Figure 3). In January, shrubs and needle forests have low FPAR values and some areas in Europe (such as Ireland, southern United Kingdom, Spain and France), Southeast Asia and the Southeastern United States with evergreen vegetation have FPAR values of about 0.5. In the mid-spring season (April), more vegetation turns green and FPAR begins to increase, especially for the area in the eastern part of the west coast of the United States, Europe (8°W–30°E; 35°N–60°N) and central and eastern China (because of planted winter wheat). In July, the greatest change happens in parts of Canada and Russia with large deciduous forests, and FPAR values reach their peak for that vegetation type (most are larger than 0.7). In October, the FPAR value in the Northern Hemisphere is a little larger than that in April, especially south of the Himalayas and in Southeast Asia.

The seasons in the Southern Hemisphere are opposite to those in the Northern Hemisphere. In some areas in South America (15°S–55°S), the largest FPAR values appear in January and minimum values in July. These regular periodic variations are also seen in Canberra and Tasmania, Australia; between 5°S and 35°S latitude in Africa; and in New Zealand.

The mean monthly hemispheric average FPAR for each land cover type from 1982 to 2006 revealed a strong seasonal pattern (Figure 4). Apart from evergreen broadleaf forest, where averaged FPAR values remain about 0.4, the peak of mean FPAR values across the Northern Hemisphere for all land cover types occurs in July. In the Southern Hemisphere, however, the maximum FPAR values are observed in January and the seasonal variations show the lowest values in the local winter in July. Because of the larger LAI values for forest vegetation, FPAR values of forest are higher than those of non-forest vegetation for both hemispheres.

In addition, the seasonal variation of FPAR of cropland in the Southern Hemisphere is not clear. Due to different planting seasons and agricultural practices, the seasonal variation of crop FPAR in three continents in the Southern Hemisphere was compared in Figure 5, showing that the FPAR values of crops reach a maximum in February, May and September for South America, Africa and Asia-Pacific in the Southern Hemisphere, respectively. Therefore, the average crop FPAR in the Southern Hemisphere cancels the peak values and makes the seasonal variation curve of seasonal fluctuations flatter than that of the Northern Hemisphere (Figure 4).

3.3 Time series patterns

The time series of 0.7° latitude zone averages of half-monthly mean FPAR over the 25-year period (January 1982 to December 2006) are shown in Figure 6. It was found that there were regular periodic variations for both hemispheres. According to the vegetation type distribution, most of the land between 30°N and 80°N is covered by deciduous forest, shrub, grass and crop. All of those vegetation types have strong seasonal patterns, and where mixed latitude-zonal average FPAR variation showed a single-peak curve for every year from 1982 to 2006, the maximum latitude-zonal mean FPAR values of about 0.8 occur during the summer period (Figure 6). However, an anomalous change was observed from the end of 1994 to the beginning of 1995, which is in agreement with Tucker *et al.* (2005): 'We began using NOAA-9

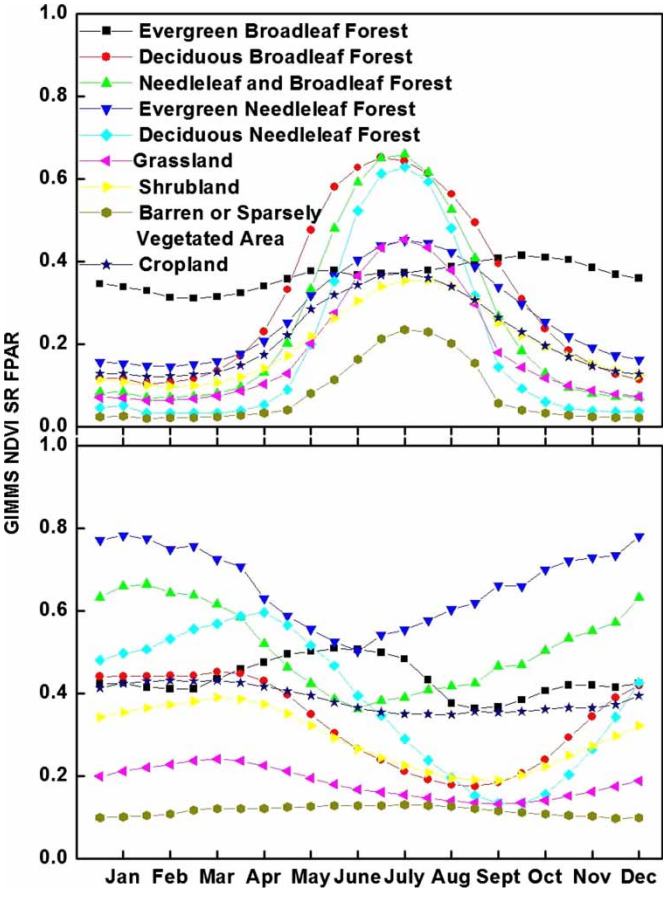

Figure 4. Seasonal variation in the monthly average FPAR across all vegetation types from 1982 to 2006 in the Northern (top) and Southern (bottom) Hemispheres.

descending node AVHRR data for our global NDVI dataset in August 1994, and continued using these data until NOAA-14 became operational in late January 1995' (Tucker *et al.* 2005).

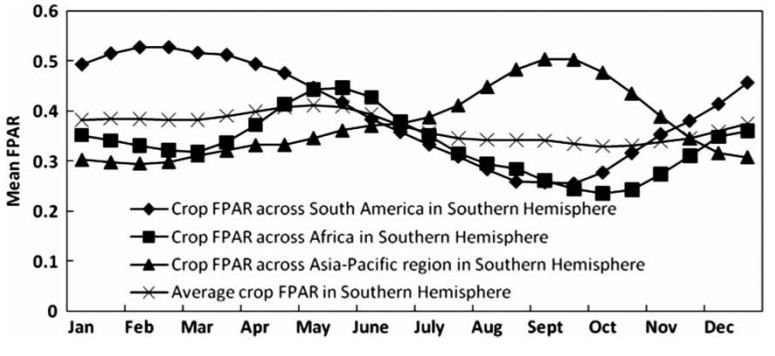

Figure 5. Seasonal variation in the monthly average FPAR of crops from 1982 to 2006 in South America, Africa and Asia-Pacific in the Southern Hemisphere.

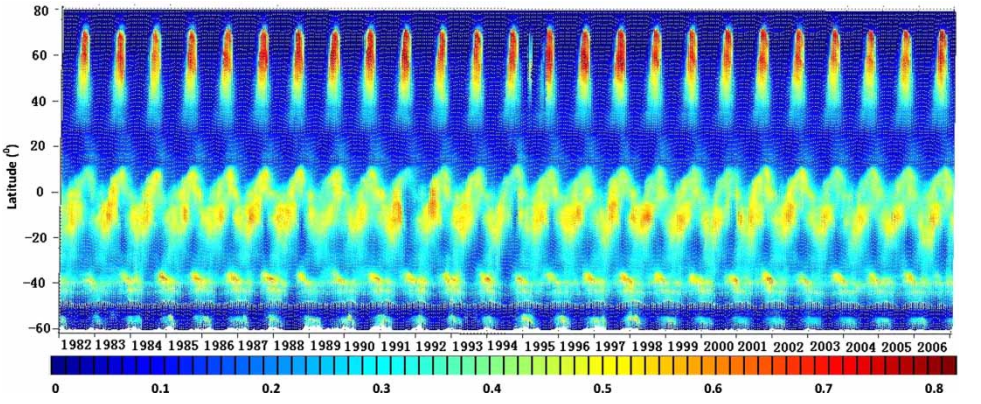

Figure 6. Time-series of 0.7° latitude zonal averages of half-monthly mean FPAR from January 1982 to December 2006.

Additionally, there is an exception for crop FPAR time series patterns in some regions because of different agricultural practices. Due to environmental and socio-economic conditions, multiple-crop systems (planting crops two or more times on the same field in one year) are quite variable throughout the world, particularly in Asia (Peng *et al.* 2011). For example, at the crop site located at 32.601°N, 114.489°E, the observed FPAR time series from 1982 to 2006 showed a double-peak curve each year (Figure 7) because of double-cropping each year. Nevertheless, the single cropping system is dominant in middle and high latitudes in the Northern Hemisphere. For the region between 10°N and 30°N, the primary land cover is barren and sparse desert in Africa, and Asia features different cropping systems with different seasonal curves, which cancels the peak values of seasonal variation curves when averaged. Therefore, latitude-zonal averages of half-monthly mean FPAR values over the 25-year period are very low, but small seasonal variations still exist, and the maximum FPAR (about 0.38) appears in the July period (Figure 6). The same phenomenon is observed between 20°S and 30°S, where maximum FPAR appears in January (Figure 6).

For the tropical regions near the Equator, the time series from 1982 to 2006 shows an almost stable FPAR of 0.55 in all seasons, with a small fluctuation due to some shrub and sparse vegetation in Africa and the alternation of dry and wet seasons (Figure 6). The evergreen vegetation distribution extending from the Equator

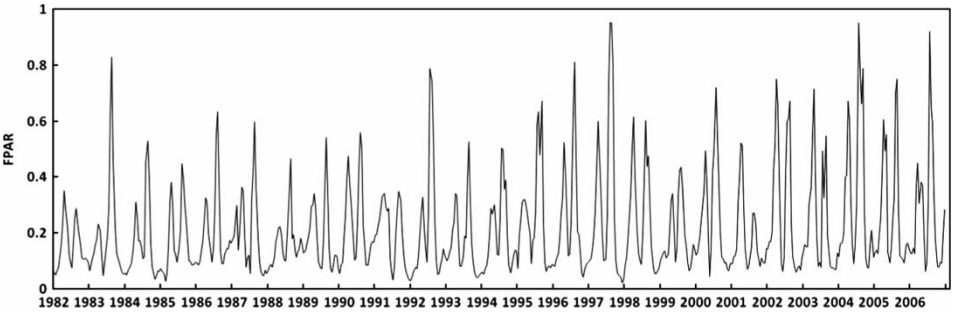

Figure 7. Time-series of half-monthly mean FPAR from January 1982 to December 2006 in a crop site (32.601389°N, 114.488611°E) with double cropping systems.

to 25°S, and even between 35°S to 55°S in Southeast Australia and Southwest South America, results in time series fluctuations of FPAR that are not as clear in the Southern Hemisphere compared to the Northern Hemisphere. However, the maximum FPAR is still observed in January (Figure 6). In addition, although there are some inter-annual patterns in FPAR, these cannot be clearly seen in the curves in Figure 6 because of the extended scale of values.

3.4 Climatic influence on global FPAR

According to the correlation coefficients between monthly climate factors and estimated FPAR, we found that both temperature and precipitation showed a significant positive correlation ($P < 0.01$) with FPAR time series variation in most meteorological stations, especially for the mid-high latitudes in the northern hemisphere (Figures 8 and 9). This indicated that temperature and precipitation act together to affect the physiological and ecological status of plants. However, some stations in the tropical rainforest in Africa, the southern part of South America and India, where the time series variations of FPAR have a negative or insignificant correlation with temperature, reflect that the seasonal cycle of FPAR follows precipitation because of the water stress in these areas. The high temperature increases evapotranspiration, which leads to more serious water stress, limiting vegetation growth and resulting in a generally negative temperature FPAR correlation in these regions. In contrast, the precipitation showed a significant positive correlation with FPAR at the level of 0.01 in these areas (Figures 8 and 9), apart from India. According to the global land cover distribution in Figure 2, most of India is covered by crops. For paddy rice in particular, manmade irrigation systems disturb the correlation between precipitation and vegetation growth.

4. Conclusions

We presented a long-term time series global FPAR product using AVHRR GIMMS NDVI from 1982 to 2006, and combined the spatial and time series of FPAR to

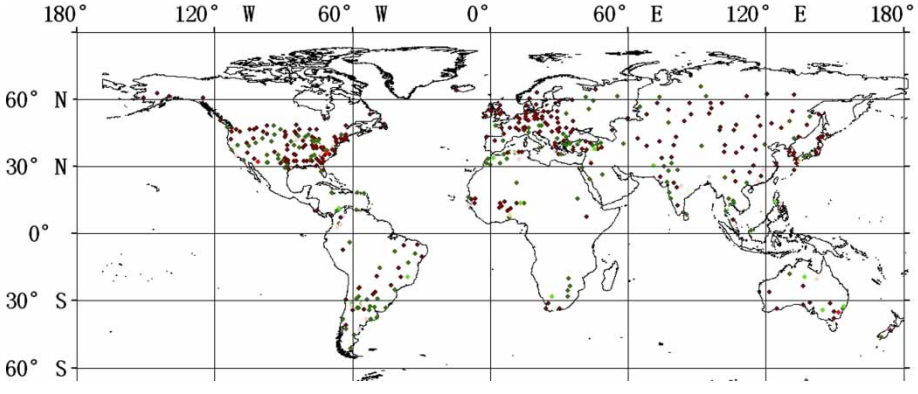

Figure 8. The significant negative (or positive) correlation level (SNCL or SPCL for short) between time series variation of monthly mean FPAR and temperature over more than 20 years from January 1982 to December 2006.

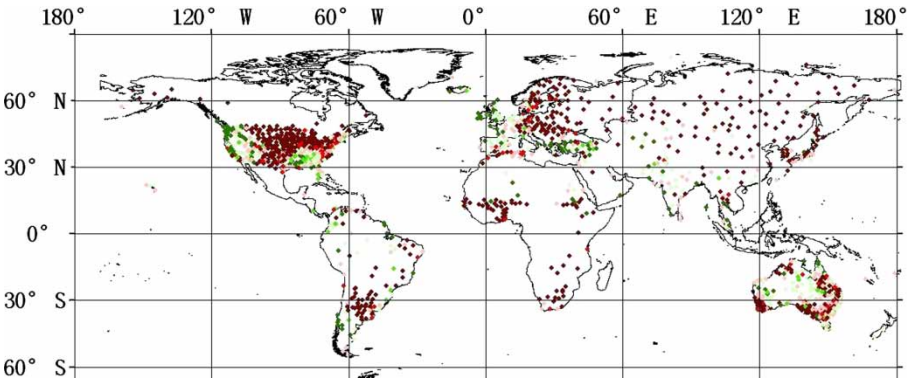

Figure 9. The significant negative (or positive) correlation level (SNCL or SPCL for short) between time series variation of monthly mean FPAR and monthly accumulated precipitation over more than 20 years from January 1982 to December 2006.

provide a comprehensive analysis of seasonal patterns of global FPAR. In addition, the main climatic factors were analysed to explore their driving mechanism on the temporal tendency of FPAR.

The FPAR estimation method was adopted from Sellers' *et al.* (1996) research on different vegetation types, and the results showed agreement between seasonal variation and MODIS FPAR in the study area (Eurasia). MODIS FPAR values were larger than GIMMS NDVI SR FPAR, especially for forest vegetation (Figure 2). With a global scale and a longer time scale, our study found that there were interrelations between spatial and seasonal patterns of FPAR. The spatial patterns of FPAR vary with vegetation type distribution and seasonal cycles (Figure 3); FPAR values for forests are higher than those of non-forest vegetation, and the maximum and minimum FPAR were observed in local summer and winter, respectively. The exception was evergreen vegetation (Figure 4), such as the area within about 5° latitude of the Equator, where FPAR values generally remain around 0.7 (Figure 3). The time series of average FPAR revealed a strong seasonal pattern, and there were regular periodic variations from January 1982 to December 2006 (Figure 6). There were large areas covered by deciduous vegetation (mainly deciduous broadleaf and needleleaf forest) in middle and high latitudes in the Northern Hemisphere, where FPAR had a considerable change from April to July, and a single-peak curve was clearly observed between 30°N and 80°N (Figure 6). Due to a large latitudinal range of evergreen vegetation distribution in the Southern Hemisphere, the average FPAR time series fluctuations in the 0.7° latitude zone were not obvious compared to those in the Northern Hemisphere (Figure 6). Moreover, the multiple-crop systems with different planting seasons worldwide had smoother seasonal FPAR variation curves averaged in the 0.7° latitude zone, especially for regions with large areas of cropland. In addition, because of the opposite seasons between the Northern and Southern Hemispheres, the peak in mean FPAR values across the Northern Hemisphere for all land cover types occurred in July. In the Southern Hemisphere, the maximum FPAR values were observed in January; the seasonal variations show the lowest values in the local winter in July (Figure 6).

Fraction of absorbed photosynthetically active radiation represents the fraction of PAR absorbed by the green plants and brown plants and is linked closely to the maximum photosynthetic capacity of vegetation (Liu *et al.* 2006). Therefore, all factors related to vegetation cover, plant growth change and plant photosynthesis will contribute to the change of FPAR. We examined the relations between the seasonal variation of climate factors (temperature and precipitation) and that of FPAR over the station locations. We found that a significant positive correlation ($P < 0.01$) was observed in most of the stations, especially for the mid-high latitudes in the Northern Hemisphere at the seasonal scale (Figures 8 and 9), which indicated temperature and precipitation act together to affect plant growth.

A major limitation in this study is underestimation of FPAR for forests; this may be attributed to the saturation of NDVI for dense vegetation. However, the available method of FPAR estimation based on NDVI developed by Sellers *et al.* (1996) was widely used, and it seems the best option to calculate FPAR using the relationship of FPAR with NDVI, especially for all vegetation types at the global scale. We estimated FPAR by the MODIS backup look-up table (LUT) in Eurasia, and found that the estimated FPAR values are even higher than the MODIS FPAR product, especially for forests. In addition, the MODIS backup LUT provides six biome classifications—less than the nine in Sellers *et al.* (1996). Therefore, we selected the method developed by Sellers *et al.* (1996) to estimate global FPAR using AVHRR GIMMS NDVI from 1982 to 2006. However, the estimation FPAR values of forests in this study are still higher than those of non-forest vegetation; the underestimation of FPAR compared to the MODIS FPAR product will not create barriers for the purpose of this study (with a focus on the seasonal tendency of FPAR). Future research should study the inter-annual change of FPAR and its driving factors, including climate change and land cover changes (afforestation, deforestation, fire disaster, urban expansion and so on).

Acknowledgements

This research was primarily funded by the National Basic Research Program of China (contract: 2009CB723902), Key Project of Digital Earth Science Platform CEODE (contract: Y01002101A), National Natural Science Foundation of China (contract: 41001205/D0106). The authors acknowledge the following data support: the AVHRR GIMMS NDVI from Global Land Cover Facility (GLCF); Globcover products from European Space Agency (ESA) and the ESA Globcover Project led by Medium Resolution Imaging Spectrometer Instrument (MERIS) France; temperature, precipitation from National Climatic Data Center (NCDC); MODIS FPAR product from the Warehouse Inventory Search Tool provides access to a complete data record of all MODIS and ASTER products available from the LP DAAC, respectively.

Notes on contributors

Dailiang Peng received his MS and PhD in Agricultural Remote Sensing from Zhejiang University. Now he is an assistant professor at the Center for Earth Observation and Digital Earth, Chinese Academy of Sciences (CAS). His current research interests include vegetation quantitatively remote sensing, and spatiotemporal analysis of remotely sensed data. He has published more than 15 journal papers.

Bing Zhang, is the Deputy Director of the Center for Earth Observation and Digital Earth, Chinese Academy of Sciences. He received his MS and PhD in Remote Sensing from the Institute of Remote Sensing Applications, CAS. He specialises in Hyperspectral Remote Sensing and has more than 17 years of experience in studying and graduate education in this field. His study interests include development of physics-based models and image processing software for the use of hyperspectral remote sensing data in solving problems in geology, hydrology, ecology and botany. Some of Dr. Bing Zhang's innovative research and research-based development projects have earned him several Chinese National, Ministerial and Provincial S&T progress awards.

Liangyun Liu is a research professor at the Center for Earth Observation and Digital Earth, CAS. He received his PhD in optics from Xi'an Institute of Optics and Precession Mechanics, CAS, in 2000. He is the author of more than 100 journal papers. His current research interests include fluorescence remote sensing, vegetation quantitatively remote sensing, and spatio-temporal analysis of remotely sensed data.

Dongmei Chen is an associate professor in Queen's University, Canada. She received her MS in GIS and remote sensing application from the Institute of Remote Sensing Application, Chinese Academic of Science, and her PhD in Geography from the joint doctoral program of San Diego State University and University of California at Santa Barbara. Her research areas focus on the understanding and modelling of interactions between human activities and the physical environment by using GIS and remote sensing techniques and spatial modelling approaches from local to regional scales.

Hongliang Fang is a research professor at the Institute of Geographic Sciences and Natural Resources Research, CAS. He received his PhD in Quantitative Remote Sensing from the Department of Geography, University of Maryland, College Park, in 2003. His main research interests include retrieval of land surface parameters from remote sensing data and assimilation of remote sensing data with crop growth model for crop yield estimation.

Yong Hu is a PhD student at the Center for Earth Observation and Digital Earth, CAS. His research interests include vegetation quantitatively remote sensing and remote sensing data processing.

References

Bacour, C., *et al*., 2006. Neural network estimation of LAI, fAPAR, fCover and LAI × Cab, from top of canopy MERIS reflectance data. Principles and validation. *Remote Sensing of Environment*, 105, 313–325.

Bicheron, P., *et al*., 2008a. *Globcover products description and validation report* [online]. European Space Agency. Available from: http://ionia1.esrin.esa.int/docs/GLOBCOVER_Products_Description_Validation_Report_I2.1.pdf [Accessed 6 July 2010].

Bicheron, P., *et al.*, 2008b. Geo-location assessment of MERIS Globcover ortho-rectified products. *Proceedings of MERIS-AATSR workshop*, September 2008, Frascati, Italy: ESA, SP–666.

Buermann, W., *et al*., 2002. Analysis of multiyear global vegetation index data set. *Journal of Geophysical Research*, 107 (D22), 4646.

Cohen, W.B., *et al*., 2003. Comparisons of land cover and LAI estimates derived from ETM+ and MODIS for four sites in North America. A quality assessment of 2000/2001 provisional MODIS products. *Remote Sensing of Environment*, 88, 233–255.

D'Arrigo, R.D., *et al*., 2000. Correlation between maximum latewood density of annual tree rings and NDVI based estimates of forest productivity. *International Journal of Remote Sensing*, 21 (11), 2329–2336.

Davenport, M.L. and Nicholson, S.E., 1993. On the relation between rainfall and the normalized difference vegetation index for diverse vegetation types in east Africa. *International Journal of Remote Sensing*, 14 (12), 2369–2389.

El Saleous, N.Z., *et al*., 2000. Improvements in the global biospheric record from the Advanced Very High Resolution Radiometer (AVHRR). *International Journal of Remote Sensing*, 21, 1251–1277.

Fang, H., *et al*., 2005. Biophysical characteristics and management effects on semiarid rangeland observed from Landsat ETM+ data. *IEEE Transactions on Geoscience and Remote Sensing*, 43 (1), 125–134.

Fensholt, R., 2004. Earth observation of vegetation status in the Sahelian and Sudanian West Africa. Comparison of Terra MODIS and NOAA AVHRR satellite data. *Remote Sensing of Environment*, 25 (9), 1641–1659.

Fensholt, R., Sandholt, I., and Rasmussen, M.S., 2004. Evaluation of MODIS LAI, fAPAR and the relation between fAPAR and NDVI in a semi-arid environment using in situ measurements. *Remote Sensing of Environment*, 91, 490–507.

Gao, B.C., 2000. A practical method for simulating AVHRR-consistent NDVI data series using narrow MODIS channels in the 0.5–1.0 mu m spectral range. *IEEE Transactions on Geoscience and Remote Sensing*, 38 (4), 1969–1975.

Gobron, N., *et al*., 1999. The MERIS global vegetation index (MGVI). Description and preliminary application. *International Journal of Remote Sensing*, 20 (9), 1917–1927.

Gobron, N., *et al.*, 2006. Evaluation of fraction of absorbed photosynthetically active radiation products for different canopy radiation transfer regimes. Methodology and results using joint research center products derived from SeaWiFS against ground-based estimations. *Journal Geophysical Research*, 111 (D13110), 1–15.

Hanan, N.P., Prince, S.D., and Bégué, A., 1995. Estimation of absorbed photosynthetically active radiation and vegetation net production efficiency using satellite data. *Agricultural and Forest Meteorology*, 76, 259–276.

Hatfield, J.L., Asrar, G., and Kanemasu, E.T., 1984. Intercepted photosynthetically active radiation estimated by spectral reflectance. *Remote Sensing of Environment*, 14, 65–75.

Huemmrich, K.F., *et al*., 2005. Time series validation of MODIS land biophysical products in a Kalahari Woodland, Africa. *International Journal of Remote Sensing*, 26 (19), 4381–4398.

Huete, A.R., 1988. A soil-adjusted vegetation index (SAVI). *Remote Sensing of Environment*, 25, 295–309.

Le Roux, X., *et al*., 1997. Radiation absorption and use by humid savannah grassland. Assessment using remote sensing and modelling. *Agricultural and Forest Meteorology*, 85, 117–132.

Liu, Z.Y., *et al*., 2006. Assessing global vegetation–climate feedbacks from observations. *Journal of Climate*, 19, 787–814.

Llewellyn, L.M., 2004. *Environmental factors that affect range plant growth, 1892–2003*. [online]. Dickinson Research Extension Center. Available from: http://www.ag.ndsu.nodak.edu/dickinso/research/2003/range03e.htm [Accessed 6 August 2010].

Malmstrom, C.M., *et al*., 1997. Interannual variation in global-scale net primary production. Testing model estimates. *Global Biogeochemical Cycles*, 11 (3), 367–392.

McCallum, I., *et al*., 2010. Comparison of four global FAPAR datasets over northern Eurasia for the year 2000. *Remote Sensing of Environment*, 114, 941–949.

Monteith, J.L., 1972. Solar radiation and productivity in tropical ecosystems. *Journal of Applied Ecology*, 9, 747–766.

Myneni, R.B., *et al*., 1995. The interpretation of spectral vegetation indexes. *IEEE Transactions on Geoscience and Remote Sensing*, 33 (2), 481–486.

Myneni, R.B., *et al*., 2002. Global products of vegetation leaf area and fraction absorbed PAR from year one of MODIS data. *Remote Sensing of Environment*, 83, 214–231.

Myneni, R.B., Nemani, R.R., and Running, S.W., 1997. Estimation of global leaf area index and absorbed par using radiative transfer models. *IEEE Transactions on Geoscience and Remote Sensing*, 35, 1380–1393.

Nagol, J.R., Vermote, E.F., and Prince, S.D., 2009. Effects of atmospheric variation on AVHRR NDVI data. *Remote Sensing of Environment*, 113, 392–397.

Nemani, R.R., *et al*., 2003. Climate driven increases in global terrestrial net primary production from 1982 to 1999. *Science*, 300, 1560–1563.

Notaro, M., Liu, Z., and Williams, J.W., 2006. Observed vegetation–climate feedbacks in the United States. *Journal of Climate*, 19, 763–786.

Peng, D.L., *et al*., 2008. Assessing the response of seasonal variation of net primary productivity to climate using remote sensing data and geographic information system techniques in Xinjiang. *Journal of Integrative Plant Biology*, 50 (12), 1580–1588.

Peng, D.L., *et al*., 2010. Spatial and seasonal characterization of net primary productivity and climate variables in southeastern China using MODIS data. *Journal of Zhejiang University-SCIENCE B (Biomedicine & Biotechnology)*, 11 (4), 275–285.

Peng, D.L., *et al*., 2011. Detection and estimation of mixed paddy rice cropping patterns with MODIS data. *International Journal of Applied Earth Observation and Geoinformation*, 13, 13–23.

Peterson, T.C., *et al*., 1998. Global historical climatology network (CHCN) quality control of monthly temperature data. *International Journal of Climatology*, 18, 1169–1179.

Peterson, T.C. and Vose, R.S., 1997. An overview of the global historical climatology network temperature database. *Bulletin of the American Meteorological Society*, 78 (12), 2837–2849.

Potter, C.S., Klooster, S.A., and Brooks, V., 1999. Interannual variability in terrestrial net primary production. Exploration of trends and controls on regional to global scales. *Ecosystems*, 2, 36–48.

Ruimy, A., Saugier, B., and Dedieu, G., 1994. Methodology for the estimation of terrestrial net primary production from remotely sensed data. *Journal of Geophysical Research*, 99 (D3), 5263–5283.

Sellers, P.J., *et al*., 1992. Canopy reflectance, photosynthesis, and transpiration. III. A reanalysis using improved leaf models and a new canopy integration scheme. *Remote Sensing of Environment*, 42 (3), 187–216.

Sellers, P.J., *et al*., 1996. A revised land surface parameterization (SiB2) for atmospheric GCMs. Part II. The generation of global fields of terrestrial biophysical parameters from satellite data. *Journal of Climate*, 9, 706–737.

Tucker, C.J., *et al*., 2005. An extended AVHRR 8-km NDVI data set compatible with MODIS and SPOT vegetation NDVI data. *International Journal of Remote Sensing*, 26 (20), 4485–4498.

Wang, Y., *et al*., 2004. Evaluation of the MODIS LAI algorithm at a coniferous forest site in Finland. *Remote Sensing of Environment*, 91, 114–127.

Wang, J., Rich, P.M., and Price, K.P., 2003. Temporal responses of NDVI to precipitation and temperature in the central Great Plains, USA. *International Journal of Remote Sensing*, 24 (11), 2345–2364.